Journal of Peptide Science
J. Pept. Sci. 2006; **12**: 612–619
Published online 13 June 2006 in Wiley InterScience (www.interscience.wiley.com). DOI: 10.1002/psc.769

JOURNAL OF PEPTIDE SCIENCE

Cyclodecapeptides to mimic the radical site of tyrosyl-containing proteins

MOHAMMED AKHTER HOSSAIN,[a,b] FABRICE THOMAS,[a]* SYLVAIN HAMMAN,[a] ERIC SAINT-AMAN,[c] DIDIER BOTURYN,[d] PASCAL DUMY[d] and JEAN-LOUIS PIERRE[a]

[a] Laboratoire de Chimie Biomimétique, LEDSS, UMR CNRS 5616, ICMG FR CNRS 2607, Université J. Fourier, BP 53, 38041, Grenoble Cedex 9, France
[b] Howard Florey Institute, University of Melbourne, Parkville, VIC 3010, Australia
[c] LEOPR, UMR CNRS 5630, ICMG FR CNRS 2607, Université J. Fourier, BP 53, 38041 Grenoble Cedex 9, France.
[d] Laboratoire d'Ingénierie Moléculaire et Chimie Bioorganique, LEDSS, UMR CNRS 5616, ICMG FR CNRS 2607, Université J. Fourier, BP 53, 38041, Grenoble Cedex 9, France

Received 14 March 2006; *Revised 12 April 2006*; *Accepted 18 April 2006*

Abstract: Tyrosyl radicals are involved in many biologically important processes. The development of model compounds to mimic radical enzyme active sites, such as galactose oxidase (GO), has widely contributed to an enhanced understanding of their spectral properties, structural attributes and even reactivity. An emerging approach towards the synthesis of such active site mimetics is the use of peptidic ligands. The potential of cyclodecapeptides to bear phenoxyl radicals has been evaluated through three compounds. $\mathbf{LH_4}^{2+}$ is a cyclodecapeptide containing two histidine residues (mimicking His_{496} and His_{581} of GO) and two tyrosine residues (mimicking Tyr_{495} and the $Tyr_{272}^{\bullet}$ radical of GO). $\mathbf{L^{tBu}H_4}^{2+}$ and $\mathbf{L^{OMe}H_4}^{2+}$ incorporate 2,4,6-protected phenols in place of each tyrosine in $\mathbf{LH_4}^{2+}$. The deprotonation constants of each peptide determined by potentiometric titrations showed that there are some interactions between the acido-basic residues. Cyclic voltammetric studies revealed that only the peptides incorporating 2,4,6-protected phenolates exhibit reversible redox couples and are thus precursors of radicals stable enough to persist in solution. These studies also showed $\mathbf{L^{OMe2-}}$ to possess the lower oxidation potential, indicating that this peptide, in its radical form, is the most stabilized. The electrochemically generated radical species have been characterized by EPR spectroscopy.

Keywords: phenol; phenoxyl; radical; RAFT; cyclic decapeptide

INTRODUCTION

Tyrosyl radicals are the focus of increasing interest owing to their involvement in many biologically important processes [1,2]. They are proposed to play a crucial role in electron and/or proton transfer. The local protein environment is expected to exert a considerable influence on the physicochemical properties of the radical itself. In photosystem II, the tyrosyl oxygen hydrogen bonds to the proton of a neighbouring histidine residue [3–5]. Such an electrostatic environment induces a spin redistribution that affects the radical properties. On the other hand, the tyrosyl radical of galactose oxidase (GO) is coordinated to a metal: Its active site contains a copper ion coordinated to two nitrogens (from His_{496} and His_{581}) and three oxygens (from the axial Tyr_{495} and equatorial cross-linked $Tyr_{272}^{\bullet}$ plus one from the substrate), and adopts a distorted square pyramidal coordination [6,7]. The redox-active tyrosine Tyr_{272} is cross-linked to Cys_{228}, which forms a thioether bond to one of the *ortho* carbon of the phenol ring. This results in a lowering of the tyrosine oxidation potential, which has been estimated to be 0.40 V [7].

The development of model compounds to mimic metalloenzyme active sites has widely contributed to an enhanced understanding of their spectral properties, structural attributes and even reactivity. A general limitation of chemical analogues of such purposes is often their low water-solubility and the poor enantioselectivity in catalysing reactions. Moreover, structural and reactivity studies on metalloproteins have revealed that the properties of their active sites depend on more than the metal coordination sphere. Modelling the second sphere interaction is posing a new challenge to improve the biological relevance of complexes mimicking the metalloprotein active sites. An emerging and fascinating approach that accounts for all these factors is the use of oligopeptides as ligands. We apply this approach here, to develop pro-radical ligands that are designed to incorporate metal ions and thus model the active site of GO.

The copper(II) coordination chemistry of oligopeptides has been extensively studied [8–10], but much less is known about the incorporation of biologically relevant radicals in such peptides [11–13]. In this study, we used cyclic decapeptides incorporating two proline–glycine sequences to induce β-turn hairpins. The peptide conformation was then constrained into an anti-parallel β sheet [14,15] and a regioselective functionalization was achieved above the plane of this motif

*Correspondence to: F. Thomas, Laboratoire de Chimie Biomimétique, LEDSS, UMR CNRS 5616, ICMG FR CNRS 2607, Université J. Fourier, BP 53, 38041, Grenoble Cedex 9, France;
e-mail: Fabrice.Thomas@ujf-grenoble.fr

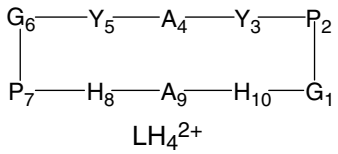

Figure 1 Formulae of $\mathbf{LH_4}^{2+}$.

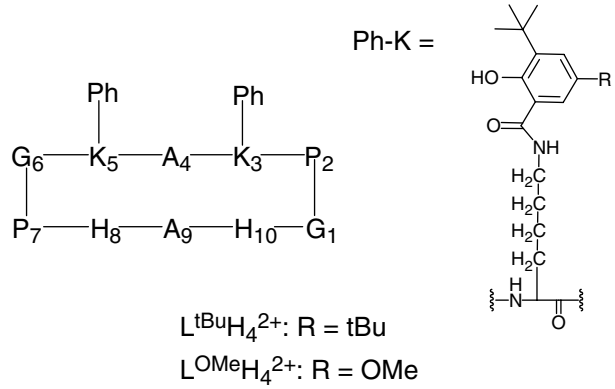

Figure 2 Formula of $\mathbf{L^{tBu}H_4}^{2+}$ and $\mathbf{L^{OMe}H_4}^{2+}$.

by amino acids at the 3,5,8 and 10th position (Figure 1). In $\mathbf{LH_4}^{2+}$ (Figure 1) the Tyr_3 and Tyr_5 residues are devoted to mimic Tyr_{495} and Tyr_{272} of GO, while His_8 and His_{10} model His_{496} and His_{581}. $\mathbf{LH_4}^{2+}$ is the simplest peptide, and will therefore be used as reference.

For phenoxyl radicals to exist as more than a transient intermediate, the *ortho* and *para* positions of the phenol must be blocked by groups, which give increased steric protection or resonance stabilization [16], as in GO [7]. Since this is not the case for the tyrosines in $\mathbf{LH_4}^{2+}$, it is not expected to be the precursor of stable phenoxyl radicals. We have therefore introduced 2,4,6-protected phenols instead of each tyrosine residue in the peptide ligands $\mathbf{L^{tBu}H_4}$ and $\mathbf{L^{OMe}H_4}$. The lysine side chains Lys_3 and Lys_5 (Figure 2) were used as addressable sites to incorporate phenols activated at one *ortho* position with a succinimide ester. The second *ortho* and remaining *para* position were substituted by electron-donating substituents, to stabilize the resulting phenoxyl radicals.

We present therein details of the synthesis and oxidative behaviour of $\mathbf{LH_4}^{2+}$, $\mathbf{L^{tBu}H_4}$ and $\mathbf{L^{OMe}H_4}$. As radicals must be generated by oxidation of phenolate groups (oxidation of phenols is known to occur at very high potentials, and is coupled to chemical reactions), the acid-base properties of each peptide are also presented.

MATERIALS AND METHODS

Generals

All chemicals were of reagent grade and used without purification. ^1H and ^{13}C NMR spectra were recorded on a Bruker AM 300 spectrometer at 300 and 75 MHz, respectively. Chemical shifts are given in ppm relative to internal standard tetramethylsilane (TMS). Mass spectra were recorded on a Thermofinnigen (EI/DCI) apparatus. RP-HPLC analyses were performed on Waters equipment. Mass spectra were recorded on electron spray ionization (ESI-MS) on a VG platform II (micromass).

Peptide

2-chlorotrityl chloride resins and protected amino acids were purchased from Advanced ChemTech Europe (Brussels, Belgium), Bachem Biochimie SARL (France) and France Biochem S. A. (France). The coupling reagent PyBOP was purchased from France Biochem and other general reagents were purchased from Aldrich and Across (France).

EPR

X-band EPR spectra were recorded on a BRUKER ESP 300E spectrometer equipped with a BRUKER nitrogen flow cryostat. Spectra were treated using the WINEPR software and simulated using the BRUKER SIMFONIA software.

Potentiometric Titrations

All measurements were performed at 25 °C and the solutions were prepared with deionized and twice distilled water. The ionic strength was fixed at $I = 0.1$ M with sodium perchlorate (PROLABO puriss.). The potentiometric titrations were performed using an automatic titrator system DMS 716 Titrino (Metrohm) with a combined glass microelectrode (Metrohm, filled with saturated NaCl solution) and connected to an IBM Aptiva microcomputer.

For measurements in water, the electrodes were calibrated to read pH according to the classical method [17]. For measurements in $CH_3CN : H_2O$ (1 : 1), the measured potentials were converted into $^{s}_{w}$pH ($^{s}_{w}$pH being the pH measurement in semi-aqueous media) using a known procedure [18]. The peptides, *ca* 0.0005 M, were titrated with 0.01 M solutions of sodium hydroxide. Argon was bubbled through the solutions to exclude CO_2 and O_2. Sodium hydroxide was freshly prepared prior to measurement. The titration data (*ca* 150 points) were refined by the non-linear least-squares refinement program SUPERQUAD [19] to determine the deprotonation constants. The pK_a values were calculated from the cumulative constants determined with the program. The uncertainties in the pK_a values correspond to the added standard deviations in the cumulative constants.

Electrochemistry

Cyclic voltammetry (CV) measurements were carried out at 298 K in *ca.* 0.4 mM solutions of each peptide. The electrolytic solutions were similar to those used for potentiometric titrations. Measurements were performed on a CHI 660 potentiostat using a conventional three-electrode electrochemical cell. A glassy carbon disc was used as a working electrode (3 mm in diameter) and a Pt wire as the secondary electrode. The reference electrode consisted of a Ag/0.01 M $AgNO_3$ system. Experiments were performed under an argon atmosphere. Electrolysis of $\mathbf{L^{2-}}$, $\mathbf{L^{tBu2-}}$ and $\mathbf{L^{OMe2-}}$ was performed

DOI: 10.1002/psc

at a carbon-felt electrode (1 × 1 × 0.5 cm) by controlled potential electrolysis, using a PAR 273 potentiostat. During this experiment, the temperature had to be maintained at 263 K to limit decomposition of the radical species. A 0.1 M $NaClO_4$ in $CH_3CN : H_2O$ (1 : 1) was used as an electrolytic solution.

General Procedure for Solid-Phase Peptide Synthesis

The side chain protected linear peptides were synthesized using manual solid-phase peptide synthesis and standard Fmoc chemistry in glass reaction vessels fitted with a sintered glass frit. Coupling reactions were performed using 1.5 equiv. of *N*-α-Fmoc protected amino acids (relative to the resin loading) activated *in situ* with 1.5–2 equiv. of PyBOP and 3–4 equiv. of diisopropylethyl amine (DIPEA) in DMF (10 ml/g resin). Coupling efficiencies were assessed by a TNBS test. The growing peptide chains were subjected to *N*-Fmoc deprotection in the presence of 20% piperidine in DMF and this process repeated three times in total to ensure complete deprotection. The success of each reaction was verified by measuring the UV absorption of piperidine washings at 299 nm. The synthetic linear peptides were cleaved from the resin using 1% TFA in DCM, treating the resin with this solution for 2 min repeatedly until the resin beads became dark purple. The combined washings were concentrated under reduced pressure and the solid white peptides were obtained by precipitation from ice-cold diethyl ether. The crude peptides were analysed by RP-HPLC and mass spectroscopy. Each linear peptide synthesized was used for cyclization without further purification.

General Procedure for Cyclization Reactions

The peptides were dissolved in DMF (0.5 mM) and the pH adjusted to 8.5 with DIPEA. PyBOP (1.2 equiv.) was added and the reaction solution stirred at room temperature for 1 h as previously reported [20]. After completion of the reaction, DMF was evaporated under reduced pressure and the residue re-dissolved in a minimum amount of DCM. The peptide was precipitated from DCM using ice-cold diethyl ether and further washed three times to remove excess reagents. The supernatant was discarded each time and the crude peptides left to air-dry. No further purification was necessary for the subsequent reactions.

Synthesis of LH_4^{2+}

A total of 195 mg (0.117 mmoles) of the fully protected linear peptide {H-His(Trt)-Ala-His(Trt)-Pro-Gly-Tyr(tBu)-Ala-Tyr(tBu)-Pro-Gly-OH} was obtained from 0.14 mmoles of resin. This crude peptide (25 mg, 0.018 mmoles) was then cyclized with PyBOP as described earlier. Final side chain deprotection was carried out in a mixture of TFA : TIS : H_2O (95 : 2.5 : 2.5) for 2 h at room temperature. After completion of the reaction, the solvent was evaporated under reduced pressure and the residue re-dissolved in a small amount of DCM. Ice-cold diethyl ether was added to precipitate the peptide as described above. The target peptide, $\mathbf{LH_4^{2+}}$, was purified by RP-HPLC and characterized by ESI-MS (found 1051.3, calcd. 1051.14). A total of 12 mg (63% overall yield estimated from the crude linear peptide) of the TFA^- salt of $\mathbf{LH_4^{2+}}$ peptide was obtained as a white powder after lyophilization. The reaction was then performed on a larger scale to produce enough peptide to perform all subsequent measurements.

Preparation of 3-*tert*-Butyl-2-hydroxy-5-methoxy-benzoic acid 2,5-dioxo-pyrrolidin-1-yl ester

Methyl 3-tert-Butyl-2-hydroxy-5-methoxy benzoate. Concentrated H_2SO_4 (20 ml) was added dropwise to a solution of methyl 2-hydroxy-5-methoxy benzoate (3.6 g, 20 mmol) and 2-methyl-2-propanol (20 ml) in methanol (4 ml) with vigorous stirring and cooling (0–5 °C). The mixture was stirred at room temperature for 5 h. The white precipitate was filtered off, washed with distilled water, dried and crystallized in methanol. Yield: 3.5 g (73%). m.p. 119–121 °C; ^{1}H NMR ($CDCl_3$) $\delta = 1.41$ (s, 9H), 3.76 (s, 3H), 3.93 (s, 3H), 7.11 (d, $J = 2, 9$ Hz, 1H), 7.6 (d, $J = 2.9$ Hz, 1H); ^{13}C NMR ($CDCl_3$) $\delta = 29.3, 35.1, 52.3, 55.7, 108.4, 111.5, 122.5, 139.7, 151.1, 156.1, 171.4$.

3-tert-Butyl-2-hydroxy-5-methoxy benzoic acid. A solution of KOH (1.2 g; 21 mmol) in water (1.5 ml) was added to methyl 3-*tert*-butyl-2-hydroxy-5-methoxy benzoate (2.50 g, 10.5 mmol) dissolved in methanol (6 ml). The mixture was heated at reflux for 5 h. After cooling (0–5 °C), the mixture was acidified with HCl 4N. The precipitate was filtered off, washed with water, treated with acetone and again filtered off. Yield: 1.7 g, (72%). m.p. 188–189 °C; ^{1}H NMR (CD_3OD) $\delta = 1.38$ (s, 9H), 3.73 (s 3H), 7.06 (d, $J = 3.1$ Hz, 1H), 7.22 (d, $J = 3.1$ Hz, 1H); ^{13}C NMR (CD_3OD) $\delta = 29.7, 35.8, 56.0, 110.4, 113.0, 122.8, 140.2, 152.5, 157.3, 174.3$; MS (DCI-$NH_3$/isobutan) 242(M + 18), 207.

3-tert-Butyl-2-hydroxy-5-methoxy-benzoic acid 2,5-dioxo-pyrrolidin-1-yl ester. 3-*tert*-butyl-2-hydroxy-5-methoxy benzoic acid (896 mg; 4 mmol) and *N*-hydroxysuccinimide (460 mg; 4 mmol) were dissolved in THF (15 ml) and DCC (824 mg; 4 mmol) was added. The reaction mixture was stirred overnight at room temperature and, after cooling; the dicyclohexylurea was removed by filtration. The filtrate was evaporated under reduced pressure. 3-*tert*-butyl-2-hydroxy-5-methoxy-benzoic acid 2,5-dioxo-pyrrolidin-1-yl ester was obtained by treatment of the crude product with chloroform and hexane. Yield: 834 mg (65%). m.p. 53–55 °C; ^{1}H NMR ($CDCl_3$) $\delta = 1.40$ (s, 9H), 2.92 (s, 4H), 3.78 (s, 3H), 7.23 (d, $J = 3.1$ Hz, 1H), 7.27 (d, $J = 3.1$ Hz, 1H), 9.96 (s, 1H); ^{13}C NMR ($CDCl_3$) $\delta = 25.7, 29.2, 35.2, 55.7, 107.1, 107.5, 125.4, 140.4, 151.7, 157.0, 166.0, 169.1$; MS (DCI-$NH_3$/isobutan) 339 (M + 18), 224, 207. Elemental analysis calcd. (%) for $C_{16}H_{19}NO_6$: C 59.81, H 5.96, N 4.36; found: C 59.65, H 6.21, N 4.15%.

3,5-di-tert-Butyl-2-hydroxy benzoic acid 2,5-dioxo-pyrrolidin-1-yl ester. This ester was prepared by a similar procedure as preceding ester but by using 3,5-di-*tert*-butyl-2-hydroxy benzoic acid [21] (750 mg; 3 mmol) and one equivalent of *N*-hydroxysuccinimide and of DCC. Yield: 645 mg (62%). m.p. 105 °C; ^{1}H NMR ($CDCl_3$) $\delta = 1.31$ (s, 9H), 1.42 (s, 9H), 2.92 (s, 4H), 7.64 (d, $J = 2.3$ Hz, 1H), 7.83 (d, $J = 2.5$ Hz, 1H), 10.10 (s, 1H); ^{13}C NMR ($CDCl_3$) $\delta = 25.7, 29.3, 31.3, 34.4, 35.3, 107.2, 123.5, 133.0, 137.9, 141.6, 159.8, 166.3, 169.1$; MS (DCI-$NH_3$/isobutan) 365 (M + 18), 250, 233. Elemental analysis calcd. (%) for $C_{19}H_{25}NO_5$: C 65.69, H 7.26, N 4.04; found: C 65.50, H 7.63, N 4.63%.

DOI: 10.1002/psc

Synthesis of $L^{tBu}H_4^{2+}$ and $L^{OMe}H_4^{2+}$

500 mg (0.33 mmoles) of the crude linear peptide {H-His(Trt)-Ala-His(Trt)-Pro-Gly-Lys(alloc)-Ala-Lys(alloc)-Pro-Gly-OH} was obtained from 505 mg of resin (1.4 mmoles/g). 200 mg (0.12 mmoles) of this linear peptide (crude) was cyclized as previously described [22]. The alloc groups on each lysine side chain were removed from the crude cyclic peptide (193 mg, 0.118 mmoles/DCM) by treatment with phenylsilane (0.728 ml, 5.9 mmoles) and $Pd(PPh_3)_4$ (27 mg, 0.0236) [20]. The reaction was carried out for 1 h at room temperature under a nitrogen environment and concentrated under reduced pressure to afford an oil. The residue was re-dissolved in a small amount of DCM and the peptide precipitated out using ice-cold diethyl ether to give 148 mg (0.1 mmoles) of crude powder. The free lysine containing peptide (74 mg, 0.05 mmoles) was then dissolved in DMF and reacted with the 3,5-di-*tert*-butyl-2-hydroxy benzoic acid 2,5-dioxo-pyrrolidin-1-yl ester (42.8 mg, 0.12 mmoles) at pH 8–9 for 1 h, to give 81 mg of crude $\mathbf{L^{tBu}H_4^{2+}}$. A second batch of this free lysine containing peptide (74 mg crude, 0.05 mmoles) was converted to $\mathbf{L^{OMe}H_4^{2+}}$ in DMF, through a reaction with the 3-*tert*-butyl-2-hydroxy-5-methoxy-benzoic acid 2,5-dioxo-pyrrolidin-1-yl ester (40 mg, 0.12 mmoles) at pH 8–9 (adjusted with DIPEA) for 1 h to give 70 mg of crude product. Deprotection of each peptide was carried out in a mixture of TFA:TIS:H_2O (95 : 2.5 : 2.5) for 2 h at room temperature to remove Trt from histidine. The final products $\mathbf{L^{tBu}H_4^{2+}}$ and $\mathbf{L^{OMe}H_4^{2+}}$ were then purified by RP-HPLC and lyophilized to give white powder ($\mathbf{L^{tBu}H_4^{2+}}$ = 17 mg, 0.0118 mmoles; $\mathbf{L^{OMe}H_4^{2+}}$ = 13 mg, 0.01 mmoles) with an overall yield 19.6% and 16.6%, respectively, that is estimated from the crude linear peptide. The peptides were characterized by ESI-MS ($\mathbf{L^{tBu}H_4^{2+}}$: calcd. 1445.6, found 1445.7; $\mathbf{L^{OMe}H_4^{2+}}$: calcd. 1393.7, found 1393.62).

RESULTS AND DISCUSSION

Peptide Synthesis

The linear decapeptides were assembled by solid-phase synthesis [23] according to an Fmoc strategy [22]. A highly acid labile linker unit, 2-chlorotrityl chloride resin, was employed to allow a side chain protected peptide to be detached from the solid support under mild conditions (1% TFA in DCM). The corresponding head-to-tail cyclization was performed in DMF under high dilution conditions (0.5 mM), utilizing PyBOP (1.2 equiv.) as a coupling reagent [20]. The Alloc moieties on lysine side-chains were removed selectively using a well-established Pd^0/PhSiH3 procedure [24], and phenol functionality was introduced using a succinimide ester of the phenol derivative (1.5 equiv. relative to each free lysine unit). Finally, all subsequent protecting groups (*t*Bu, Trt and Pmc) were removed using a cocktail solution containing TFA:TIS:H_2O (95 : 2.5 : 2.5). The target peptides $\mathbf{LH_4^{2+}}$, $\mathbf{L^{tBu}H_4^{2+}}$ and $\mathbf{L^{OMe}H_4^{2+}}$ were then purified by RP-HPLC and characterized by mass spectroscopy (ESI-MS, positive mode).

Ligand Deprotonation Constants

The ligands $\mathbf{LH_4^{2+}}$, $\mathbf{L^{tBu}H_4^{2+}}$ and $\mathbf{L^{OMe}H_4^{2+}}$ possess four deprotonation sites, two phenolic hydroxyls and two imidazoles from histidines. The deprotonation constants were determined by potentiometric titrations with NaOH of each fully protonated ligands. The titration curves of $\mathbf{LH_4^{2+}}$, $\mathbf{L^{tBu}H_4}$ and $\mathbf{L^{OMe}H_4}$ are shown in Figure 3. Analysis of the titration data using the computer program SUPERQUAD, yielded the pK_a values that are listed in Table 1.

The two higher pK_a values in each data set are assigned to deprotonation of the phenolic hydroxyls. The average deprotonation constants, $pK_{a_{av(1-2)}}$, are 9.71, 10.54 and 9.84 for $\mathbf{LH_4^{2+}}$, $\mathbf{L^{tBu}H_4^{2+}}$ and $\mathbf{L^{OMe}H_4^{2+}}$, respectively. The $pK_{a_{av(1-2)}}$ of $\mathbf{LH_4^{2+}}$ is close to that of the free tyrosine (roughly 10). Owing to a higher electron-donating effect of the methoxy group compared to that of the *tert*-butyl group, one should

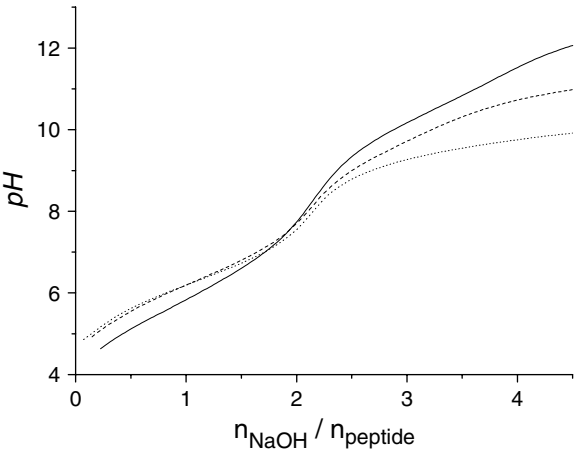

Figure 3 Potentiometric titration curves for 0.5 mM solutions of $\mathbf{LH_4^{2+}}$ (dotted lines),[a] $\mathbf{L^{tBu}H_4^{2+}}$ (solid lines)[b] and $\mathbf{L^{OMe}H_4^{2+}}$ (dashed lines)[b]. All solutions were at 298 K and ionic strength I = 0.1 M ($NaClO_4$).[a] in H_2O; [b] in H_2O : CH_3CN (1 : 1).

Table 1 Thermodynamic constants for $\mathbf{LH_4}$, $\mathbf{L^{tBu}H_4}$ and $\mathbf{L^{OMe}H_4}$ (I = 0.1 M $NaClO_4$) at 298 K

	$\mathbf{LH_4^{2+}}$[a]	$\mathbf{L^{tBu}H_4^{2+}}$[b]	$\mathbf{L^{OMe}H_4^{2+}}$[b]
$\log\beta_{1.1}$	10.46(1)	11.34(2)	10.43(1)
$\log\beta_{1.2}$	19.42(2)	21.08(3)	19.67(1)
$\log\beta_{1.3}$	26.60(2)	27.94(6)	26.52(1)
$\log\beta_{1.4}$	32.49(3)	33.33(10)	32.28(1)
pK_{a1}	10.46	11.34	10.43
pK_{a2}	8.96	9.74	9.24
pK_{a3}	7.18	6.86	6.85
pK_{a4}	5.89	5.39	5.76

[a] Determined in H_2O.
[b] Determined in the mixture H_2O : CH_3CN (1 : 1) due to the poor solubility of these peptides in H_2O.

DOI: 10.1002/psc

expect a lower $pK_{a_{av(1-2)}}$ value for $\mathbf{L^{tBu}H_4}^{2+}$ than for $\mathbf{L^{OMe}H_4}^{2+}$. This, however, is not the case and may be attributed to differences in the hydrogen bond network established between the amide and the phenol. Such an intramolecular interaction could stabilize either an amine-phenolate form (thus lowering the phenol's pK_a of $\mathbf{L^{OMe}H_4}^{2+}$) or a carbonyl-phenol form (increasing the phenol's pK_a of $\mathbf{L^{tBu}H_4}^{2+}$).

The two lower pK_a's correspond to deprotonation of the imidazole ring on each histidine residue. This process occurs with average deprotonation constants, $pK_{a_{av(3-4)}}$, of 6.54, 6.13 and 6.31. These values are roughly similar for all the three peptides, showing that the interactions between the histidine and tyrosine side chains are weak.

The range over which the determined stepwise deprotonation constants for each tyrosine (or phenol) and the histidines occur is significantly different from that of the statistical factor log 2 (0.3). This shows that there is some cooperativity between the similar acido-basic side chains within the peptide, and thus interaction, even if the linkers are flexible. The species distribution diagrams for $\mathbf{LH_4}^{2+}$, $\mathbf{L^{tBu}H_4}^{2+}$ and $\mathbf{L^{OMe}H_4}^{2+}$ are shown in Figure 4.

Oxidative Behaviour of the Ligands

The electrochemical behaviour of 0.4 mM solutions of the ligands $\mathbf{LH_4}^{2+}$, $\mathbf{L^{tBu}H_4}^{2+}$ and $\mathbf{L^{OMe}H_4}^{2+}$, were investigated by CV and differential pulse voltammetry (DPV). The electrolytic solutions were made from $H_2O:CH_3CN$ (1 : 1) containing 0.1 M $NaClO_4$. All potentials are referenced against the Ag/0.01 M $AgNO_3$ redox couple (add 0.55 V to convert from Ag/0.01 M $AgNO_3$ to the NHE scale).

For $\mathbf{LH_4}^{2+}$, CV curves were recorded in the 5.1–12.2 $^{s}_{w}$pH range. They do not exhibit any reversible signal, even in basic medium (Figure 5). This shows that either the peptides interact strongly with the electrode, or more likely still, the oxidized products were not stable over the time scale of this experiment. The DPV curves reveal a lowering of the oxidation potential while $^{s}_{w}$pH is increased, which is expected for the deprotonation of phenolic moieties ($E_p^a = 0.14$ V at $^{s}_{w}$pH = 12.2). From this experiment, one can conclude that $\mathbf{LH_4}^{2+}$ could not be considered a precursor to persistent radical species.

For $\mathbf{L^{tBu}H_4}^{2+}$, CV curves were recorded over the 5.8–12.2 $^{s}_{w}$pH range. From $^{s}_{w}$pH = 5.8 to 10, irreversible signals were observed, which is an expected result for the oxidation of phenols. A chemical reaction,

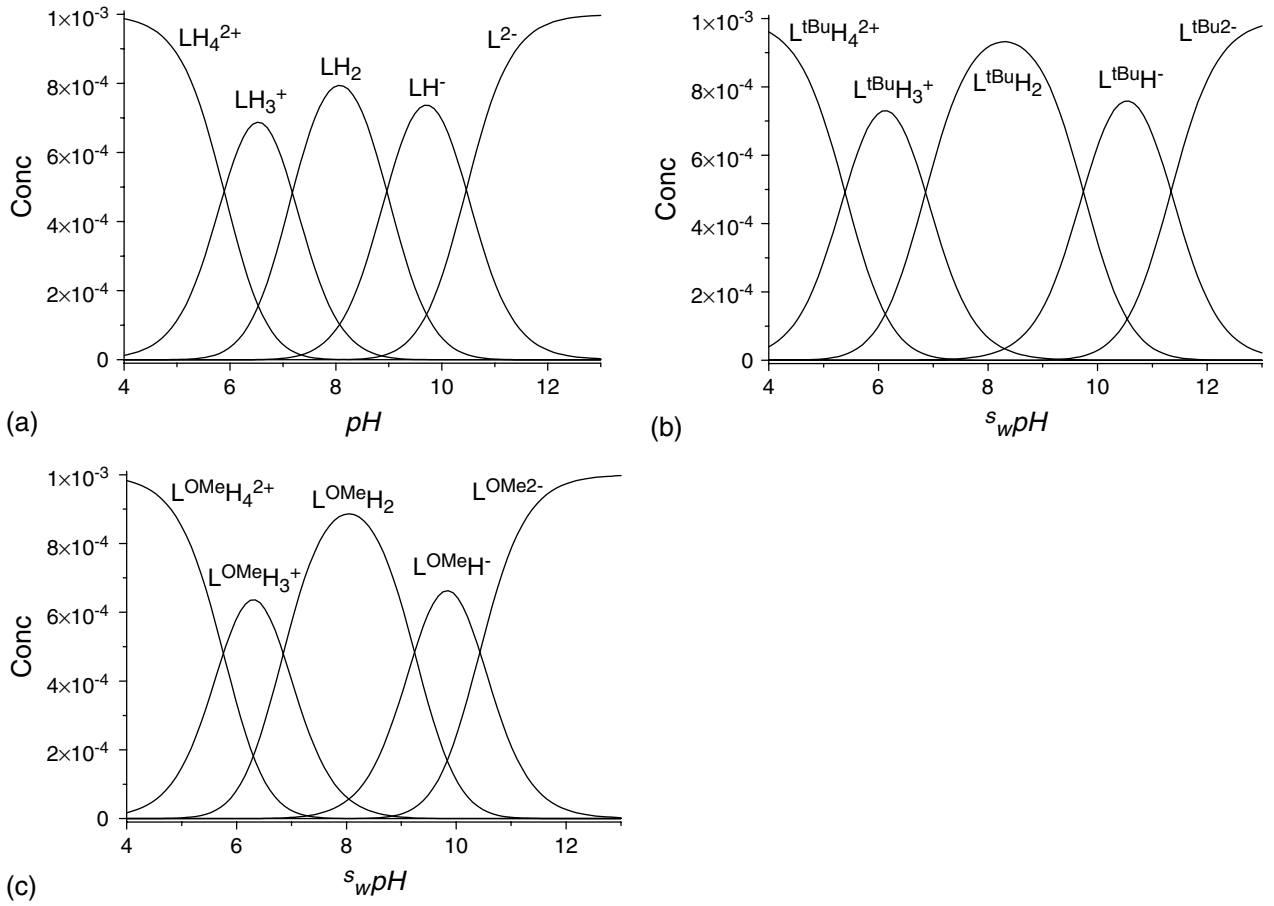

Figure 4 Species distribution diagrams for 1 mM solutions of (a) $\mathbf{LH_4}^{2+}$, (b) $\mathbf{L^{tBu}H_4}^{2+}$ and (c) $\mathbf{L^{OMe}H_4}^{2+}$ as function of pH (or $^{s}_{w}$pH), calculated with the thermodynamic constants given in Table 1.

DOI: 10.1002/psc

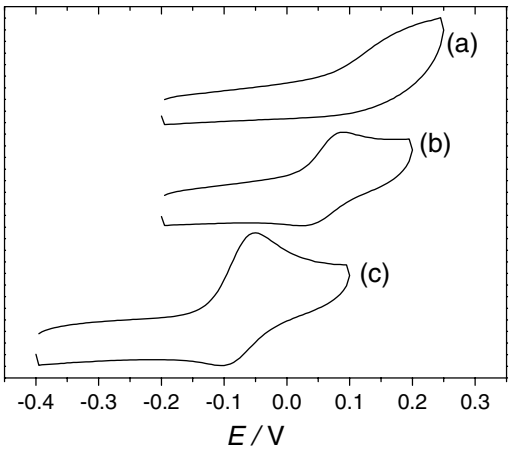

Figure 5 CV curves of 0.4 mM $H_2O:CH_3CN$ (1 : 1) solutions (+0.1 M $NaClO_4$) of (a) $\mathbf{L^{2-}}$, (b) $\mathbf{L^{tBu2-}}$, (c) $\mathbf{L^{OMe2-}}$ at ${}^{s}_{w}pH = 12.2$. Scan rate = 0.1 V.s^{-1}, $T = 298$ K. The potentials are referenced against Ag/0.01 M $AgNO_3$.

namely, proton transfer (phenoxyl radical cations are highly acidic) and/or decomposition of the radical species, is associated to the electron transfer. In contrast, a reversible signal is observed at $E_{1/2} = 0.06$ V (Figure 5) for higher ${}^{s}_{w}pH$ values (12.2). Thus, after electron transfer, the oxidized product does not evolve in basic media (over the time scale of the experiment at 298 K), showing that its stability is noteworthy.

In addition to CV curves, DPV curves were recorded over roughly the same ${}^{s}_{w}pH$ range. The DPV curve recorded at ${}^{s}_{w}pH = 5.1$ (Figure 6) revealed a broad oxidation peak at around $E_p{}^a = 0.80$ V. This corresponds to the irreversible oxidation of the phenolic moieties. When the ${}^{s}_{w}pH$ is increased, this signal progressively disappears while new oxidation peaks appear at potential values lower than 0.3 V. This is consistent with the deprotonation of the phenolic moieties: The higher electron-density at the phenolate makes it easier to oxidize. When ${}^{s}_{w}pH$ is raised from 9.0 to 10.0, the DPV curve shows an oxidation peak at $E_p{}^a = 0.23$ V whose intensity increases. This signal decreases and shifts when the ${}^{s}_{w}pH$ approaches 11.0. From the species distribution diagram of $\mathbf{L^{tBu}H_4}^{2+}$ as function of ${}^{s}_{w}pH$, it appears that at ${}^{s}_{w}pH = 9.0$, the solution consists of 83% of the phenol species $\mathbf{L^{tBu}H_2}$, and 17% of the phenol-phenolate species $\mathbf{L^{tBu}H^-}$. This ratio adjusts to 33% of $\mathbf{L^{tBu}H_2}$ and 64% of $\mathbf{L^{tBu}H^-}$ at ${}^{s}_{w}pH = 10.0$, while at ${}^{s}_{w}pH = 11.0$, the amount of $\mathbf{L^{tBu}H_2}$ becomes negligible and the solution consists of a mixture of 65% $\mathbf{L^{tBu}H^-}$ and 31% $\mathbf{L^{tBu2-}}$. The peak at $E_p{}^a = 0.23$ V is thus attributed to the oxidation of the phenolate moiety in $\mathbf{L^{tBu}H^-}$. When the ${}^{s}_{w}pH$ is increased further still, this signal is shifted towards even lower potential values and dramatically sharpens. At ${}^{s}_{w}pH = 12.2$, when the solution consists of the phenolate species $\mathbf{L^{tBu2-}}$ as the major product (88%), a sharp signal is observed at $E_p{}^a = 0.04$ V, attributed to the oxidation of both its phenolate moieties.

It is important to note that these phenolate oxidation potentials are tuned by the protonation state of the peptide. When it contains one phenol, the phenolate is oxidized at 0.23 V ($\mathbf{LH^{tBu-}}$), while when it contains two phenolates, these are oxidized at 0.04 V ($\mathbf{L^{tBu2-}}$). This shows that there are some interactions between the phenol and phenolate moieties in the partially deprotonated $\mathbf{LH^{tBu-}}$ peptide, and also that the peptide global charge (−2 *vs* −1) affects the oxidation potential. This observation could be directly correlated to the results concerning pK_a's of these phenols (described above), confirming that deprotonation of one phenol significantly influences the properties of the other. In direct contrast to this is the single peak observed for the oxidation of the two phenolates in $\mathbf{L^{tBu2-}}$. This indicates that oxidation of one phenolate moiety in the fully deprotonated peptide does not significantly affect

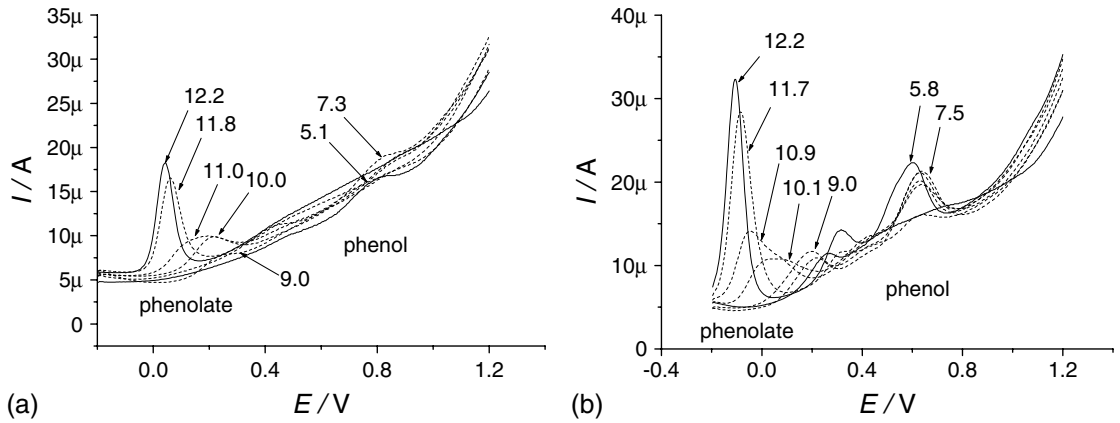

Figure 6 DPV curves of 0.4 mM $H_2O:CH_3CN$ (1 : 1) solutions (+0.1 M $NaClO_4$) of (a) $\mathbf{L^{tBu2-}}$ and (b) $\mathbf{L^{OMe2-}}$, as function of ${}^{s}_{w}pH$. The ${}^{s}_{w}pH$ values are indicated. For each series, the solid lines represent the initial and final curves (5.1 and 12.2 for $\mathbf{L^{tBu2-}}$, 5.8 and 12.2 for $\mathbf{L^{OMe2-}}$). Pulse width = 0.05 s, amplitude = 0.05 V, $T = 298$ K. The potentials are referenced against Ag/0.01 M $AgNO_3$.

DOI: 10.1002/psc

the second. The chemically equivalent phenolate units are thus electrochemically non-interacting.

$\mathbf{L^{OMe}H_4}^{2+}$ exhibits an electrochemical behaviour similar to that of $\mathbf{L^{tBu}H_4}^{2+}$ (Figures 5–6). The two main differences between $\mathbf{L^{OMe}H_4}^{2+}$ and $\mathbf{L^{tBu}H_4}^{2+}$ do, however, exist. The first concerns potential values. The phenol $\mathbf{L^{OMe}H_2}$, phenol-phenolate $\mathbf{L^{OMe}H^-}$ and phenolate $\mathbf{L^{OMe2-}}$ species exhibit $E_p{}^a$ values of 0.64, 0.20 and −0.11 V, respectively. These values are lower than the corresponding ones in $\mathbf{L^{tBu}H_4}^{2+}$. The higher electron-donating properties of methoxy groups, relative to *tert*-butyl substituents, lower the phenolate oxidation potential to values close to that reported for the oxidation of the deprotonated cross-linked Tyr_{272} in GO (−0.15 V *vs* $AgNO_3$/Ag) [7]. In addition, as shown in the DPV curves recorded at ${}^s{}_wpH = 10.9$, the contribution of each fully deprotonated peptide (at potential values lower than 0.1 V) is clearly higher for $\mathbf{L^{OMe}H_4}^{2+}$ when compared with $\mathbf{L^{tBu}H_4}^{2+}$. This suggests that the ratio $\mathbf{L^{OMe}H^-/L^{OMe2-}}$ is lower than that of $\mathbf{L^{tBu}H^-/L^{tBu2-}}$ at this ${}^s{}_wpH$ and is in perfect agreement with the species distribution diagram shown in Figure 4.

Oxidized Products

For each peptide, a controlled potential electrolysis was performed at 263 K under bubbling argon, at a carbon-felt working electrode, to generate the oxidized species (*E* applied slightly higher than the $E_p{}^a$ value obtained from DPV measurements). Electrolysis was stopped once the total charge passed corresponds to the theoretical value for two electrons removed per molecule. During this experiment, the temperature had to be maintained at 263 K, to limit decomposition of the radical species.

The 260 K X-Band EPR spectra of the electrochemically oxidized solutions of $\mathbf{L^{tBu2-}}$ and $\mathbf{L^{OMe2-}}$ are shown in Figure 7. That of $\mathbf{L^{2-}}$ did not reveal any signal, showing that these corresponding radical species is unstable, even at 263 K.

Both $\mathbf{Lox^{tBu}}$ and $\mathbf{Lox^{OMe}}$ exhibit signals centred at a g_{iso} value of 2.005, which is typical for phenoxyl radicals. The spectrum of $\mathbf{Lox^{tBu}}$ consists of a doublet, corresponding to the interaction of one hydrogen (A_H = 0.170 mT) with the electronic spin, while that of $\mathbf{Lox^{OMe}}$ is dramatically different because of the interaction of the electronic spin with each hydrogen on the methoxy substituent. The significant amount of electron-density located at this methoxy substituent is reflected by a larger hyperfine coupling constant $A_H = 0.207$ mT for 3 hydrogens giving rise to the observed four-line pattern ($2 \times n_H \times I_H = 2 \times 3 \times 1/2$ lines). Compared to the spectrum of the metal-free form of radical GO, the EPR spectra of $\mathbf{Lox^{tBu}}$ is simplified because of the loss of the strong hyperfine coupling constant with the methylene and ortho hydrogens.

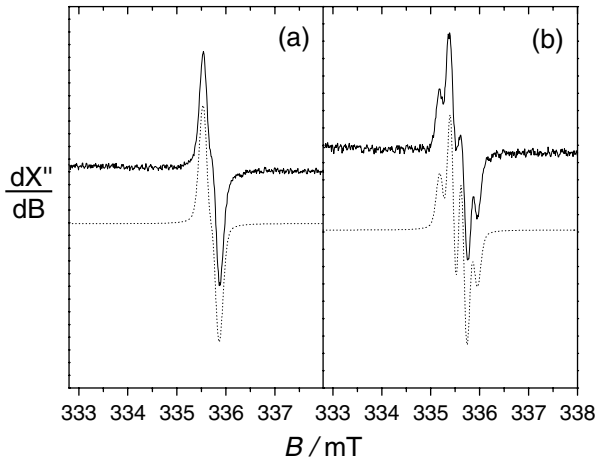

Figure 7 260 K EPR spectra of 0.4 mM $H_2O:CH_3CN$ (1 : 1) solutions (+0.1 M $NaClO_4$) of (a) $\mathbf{Lox^{tBu}}$ and (b) $\mathbf{Lox^{OMe}}$ at ${}^s{}_wpH = 12.2$. Solid lines are experimental spectra; dotted lines represent simulations using parameters given in the text. Microwave freq. = 9.42 GHz, power = 20 mW, mod. freq. = 100 KHz, amp. = 0.0784 mT.

The EPR spectra of $\mathbf{Lox^{tBu}}$ and $\mathbf{Lox^{OMe}}$ were also recorded at 100 K. Under these conditions, only broad ($S = 1/2$) signals were observed at $g = 2.005$. This indicates that the two radicals are magnetically non-interacting and that there is a large spatial separation between these units. This is not surprising as the lysine linker is flexible, but one should keep in mind that the presence of metal (a copper(II) ion in GO) may affect this spatial separation and flexibility.

CONCLUSIONS

We have shown that the tyrosyl site of radical-containing proteins could be successfully modelled using cyclodecapeptides. Potentiometric titrations revealed that interactions exist between the acido-basic residues in each of these peptides, and that the scaffold is reasonably flexible. The different oxidation behaviour observed for each peptide has been correlated to the pro-phenoxyl-like residues; $\mathbf{LH_4}^{2+}$, which contains tyrosine moieties, did not afford stable radicals. We have therefore developed a method for the chemical synthesis of peptide scaffolds presenting phenols that are protected at their 2-, 4- and 6-positions with electron-donating *tert*-butyl and methoxyl groups ($\mathbf{L^{tBu}H_4}^{2+}$ and $\mathbf{L^{OMe}H_4}^{2+}$, respectively). The electron-donating methoxy substituent allows the phenol (and phenolate) to be more easily oxidized. The radical species $\mathbf{Lox^{tBu}}$ and $\mathbf{Lox^{OMe}}$ were electrochemically generated and characterized by EPR spectroscopy. $\mathbf{Lox^{OMe}}$ differs from $\mathbf{Lox^{tBu}}$ owing to its electron-density, which is significantly delocalized over the methoxy substituent. $\mathbf{Lox^{OMe}}$ and $\mathbf{Lox^{tBu}}$ are among the first radical-peptide species that have been generated and are persistent

DOI: 10.1002/psc

enough in solution to be characterized. Since these results concern peptides containing chelating residues (histidines, amidates and phenolates), this work could open new possibilities in the design of model complexes for the copper(II) radical active site of GO. [25] The coordination chemistry of these peptides is currently in progress.

REFERENCES

1. Stubbe J, Van der Donk WA. Protein Radicals in Enzyme Catalysis. *Chem. Rev.* 1998; **98**: 705–762.
2. Fontecave M, Pierre JL. Mechanisms of formation of free radicals in biological catalysis. *C. R. Acad. Sci. Paris Chimie* 2001; **4**: 531–538.
3. Diner BA. Amino acid residues involved in the coordination and assembly of the manganese cluster of photosystem II. Proton-coupled electron transport of the redox-active tyrosines and its relationship to water oxidation. *Biochim. Biophys. Acta* 2001; **1503**: 147–163.
4. Debus RJ. Amino acid residues that modulate the properties of tyrosine YZ and the manganese cluster in the water oxidizing complex of photosystem II. *Biochim. Biophys. Acta* 2001; **1503**: 164–186.
5. Faller P, Goussias C, Rutherford AW, Un S. Resolving intermediates in biological proton-coupled electron transfer: a tyrosyl radical prior to proton movement. *Proc. Natl. Acad. Sci. U.S.A.* 2003; **100**: 8732–8735.
6. Ito N, Phillips SEV, Stevens C, Ogel ZB, McPherson MJ, Keen JN, Yadav KDS, Knowles PF. Novel thioether bond revealed by a 1.7 Å crystal structure of galactose oxidase. *Nature* 1991; **350**: 87–90.
7. Whittaker JW. Free radical catalysis by galactose oxidase. *Chem. Rev.* 2003; **103**: 2347–2363.
8. Kallay C, Varnagy K, Micera G, Sanna D, Sovago I. Copper(II) complexes of oligopeptides containing aspartyl and glutamyl residues. Potentiometric and spectroscopic studies. *J. Inorg. Biochem.* 2005; **99**: 1514–1525.
9. Kozlowski H, Bal W, Dyba M, Kowalik-Jankowska T. Specific structure-stability relations in metallopeptides. *Coord. Chem. Rev.* 1999; **184**: 319–346.
10. Kozlowski H, Kowalik-Jankowska T, Jezowska-Bojczuk M. Chemical and biological aspects of Cu2+ interactions with peptides and aminoglycosides. *Coord. Chem. Rev.* 2005; **249**: 2323–2334.
11. DeFelippis MR, Murthy CP, Broitman F, Weinraub D, Faraggi M, Klapper MH. Electrochemical properties of tyrosine phenoxy and tryptophan indolyl radicals in peptides and amino acid analogs. *J. Phys. Chem.* 1991; **95**: 3416–3419.
12. Tommos C, Skalicky JJ, Pilloud DL, Wand J, Dutton PL. De novo proteins as models of radical enzymes. *Biochemistry* 1999; **38**: 9495–9507.
13. Giese B, Napp M, Jacques O, Boudebous H, Taylor AM, Wirz J. Multistep electron transfer in oligopeptides: direct observation of radical cation intermediates. *Angew. Chem. Int. Ed.* 2005; **44**: 4073–4075.
14. Peluso S, Rückle T, Lehmann C, Mutter M, Peggion C, Crisma M. Crystal structure of a synthetic cyclodecapeptide for template-assembled synthetic protein design. *Chembiochem* 2001; **2**: 432–437.
15. Sénèque O, Crouzy S, Boturyn D, Dumy P, Ferrand M, Delangle P. Novel model peptide for Atx1-like metallochaperones. *Chem. Commun.* 2004; 770–771.
16. Altwicker ER. Chemistry of stable phenoxy radicals. *Chem. Rev.* 1967; **67**: 475–531.
17. Martell AE, Motekaitis RJ. *Determination and use of Stability Constants*, (2nd edn). VCH Publishers: New York, 1992.
18. Espinosa S, Bosch E, Roses M. Acid – base constants of neutral bases in acetonitrile – water mixtures. *Anal. Chim. Acta* 2002; **454**: 157–166.
19. Gans P, Sabatini A, Vacca A. SUPERQUAD: an improved general program for computation of formation constants from potentiometric data. *J. Chem. Soc. Dalton Trans.* 1985; 1195–1200.
20. Dumy P, Eggleston I, Servigni S, Sila U, Sun X, Mutter M. A convenient synthesis of cyclic peptides as regioselectively addressable functionalized templates (RAFT). *Tetrahedron Lett.* 1995; **36**: 1255–1258.
21. Scheuer A, Mosset P, Bauer W, Saalfrank RW. A practical route to regiospecifically substituted (*R*)- and (*S*)-Oxazolylphenols. *Eur. J. Org. Chem.* 2001; 3067–3074.
22. Atherton E, Shepard RC. *Solid Phase Peptide Synthesis: a Practical Approach*. IRL press at Oxford University Press: 1989.
23. Stewart JM, Young JD. *Solid Phase Peptide Synthesis*, (2nd edn). Pierce Chemical Co: Rockford, Illinois, 1984.
24. Thieriet N, Alsina J, Giralt E, Guibe F, Albericio F. Use of alloc-amino acids in solid-phase peptide synthesis. Tandem deprotection-coupling reactions using neutral conditions. *Tetrahedron Lett.* 1997; **38**: 7275–7278.
25. Michel F, Thomas F, Hamman S, Saint-Aman E, Bucher C, Pierre JL. Galactose oxidase models: solution chemistry and phenoxyl radical generation mediated by the copper status. *Chem. Eur. J.* 2004; **10**: 4115–4125.

DOI: 10.1002/psc